Numerical Methods in Civil Engineering, 9-3 (2025) 01-10

Numerical Methods in Civil Engineering

Journal Homepage: https://nmce.kntu.ac.ir/

Comparison of numerical methods for the solution of Richards' equation in layered porous media

Roza Asadi*, Zahra Zamani Aliabadi**

ARTICLE INFO

RESEARCH PAPER

Article history:
Received:
February 2023
Revised:
July 2023
Accepted:
July 2023

Keywords:
Numerical modelling,
Richards' equation,
Unsaturated flow,
Finite volume method,
Van Genuchten soil model

Abstract:

In this research, the advanced finite volume scheme of the Dual Discrete method has been used for the numerical modeling of Richards' equation. Three forms of Richards' equation, including head form, water content form, and mixed form with a modified Picard linearization, are developed and assessed in the two-dimensional domain. Various examples using different soil properties, boundary conditions, and grid structures are solved. The results agree very well with the analytical and numerical solutions in both homogenous and layered porous media. The different forms have been compared in terms of accuracy, the number of iterations, and mass balance ratio. For the test cases considered in this study, the water content form has been determined as the superior method due to the low mass balance error, higher accuracy, and less number of iterations. Also, the modified Picard form improves the conservation of mass and efficiency in comparison to the head-based method. The results indicate that for the head form, a small time step is required to obtain an accurate mass balance, while the two other schemes yield superior mass balance results, even for large time steps. Moreover, the proposed finite volume method shows stable solutions without any numerical oscillations for all of the test cases.

1. Inroduction

Simulation of groundwater flow in unsaturated soils is of great interest in many engineering problems, including estimating recharge in a phreatic aquifer, moisture loss in shallow water aquifers, and consequently, management of water resources [1-3]. In many unsaturated zone studies, fluid flow is assumed to follow the Richards' equation [4]. Due to the nonlinearity of the Richards' equation, analytical solutions could be obtained only under simplifying assumptions. Therefore, numerical methods are required in case of problems with complex geometries and different types of boundary conditions. In the past few decades, considerable effort has been made to develop efficient and fast schemes for solving Richards' equation [5-14]. In spite of improvements in capturing accurate and precise solutions for different types of problems, challenging issues still exist.

**Corresponding author: Assistant professor, Faculty of Civil Engineering, K. N. Toosi University of Technology, Tehran, Iran.*
Email: asadi@kntu.ac.ir
*** M.Sc. student, K. N. Toosi University of Technology, Tehran, Iran.*

The first challenge is due to the numerical oscillations occur in the methods such as finite difference and finite element methods [5, 8, 15-17]. In this research, the finite volume method (FVM) has been used for numerical modeling; since studies show that this method is introduced to achieve high-order accuracy, reduces errors, avoids numerical oscillation, and preserves mass conservation at the element level [10,11,13,14,18-23]. Among different types of FVMs, the dual discrete finite volume method (DDFVM) has been developed to model Richards' equation in two dimensional domain. Since in the so-called method, the flux is computed with more than two points, and can handle unstructured grids, is well-suited for heterogeneous and anisotropic porous media [20-23]. This numerical scheme is successfully applied for the saturated flow in highly heterogeneous reservoirs [22].

In addition to the type of numerical method applied for the discretization, the form of Richards' equation could affect the accuracy and convergence of the solution [5, 8, 24]. Based on the type of variable used in the Richard's

https://doi.org/10.61186/NMCE.2302.1007

equation, three forms, including water content (θ) −based form, pressure head (h) −based form and mixed form could be obtained.

The studies show that the θ −based form may exhibit numerical difficulties in heterogeneous and saturated-unsaturated soils, while the h −based form is more versatile. On the other hand, the h −based form may lead to large mass balance errors compared to the θ −based form [8, 9, 25-27]. In this context, the modified Picard method has been proposed in [8] to combine the advantages of both methods. However, the truncation errors would exist in the Taylor series of the time derivative of water content. Based on many studies conducted in this research field, no single form could be adapted for all kinds of problems in unsaturated porous media. It should be noted that the mechanical stress state variables are not considered, and the work is focused on hydraulics analysis because these parameters considerably impact the results.

According to the issues mentioned above, in this study, the stability, accuracy, and efficiency of the DDFVM have been investigated through different forms of Richards' equation.

This paper is organized as follows: the mathematical formulation has been presented in section 2, the numerical model of DDFVM has been proposed in section 3, the numerical model has been validated in section 4, and different methods are compared via various examples, and finally conclusions are reached in section 5.

2. Mathematical formulations

The Richards' equation for modelling the water flow in unsaturated porous media could be obtained by combining the mass conservation law with the generalized Darcy's law [4]. This equation can be formulated in three forms, including the mixed form (Equation 1), the head-based (h-based) form (Equation 2), and the water-content-based (θ-based) form (Equation 3). These equations in 3D can be written as follows:

$$\frac{\partial \theta}{\partial t} = \nabla\left[K(h)\nabla(h+z)\right] \tag{1}$$

$$C(h)\frac{\partial h}{\partial t} = \nabla\left[K(h)\nabla(h+z)\right] \tag{2}$$

$$\frac{\partial \theta}{\partial t} = \nabla[D(\theta)\nabla\theta] + \nabla K(\theta) \tag{3}$$

in the above equations, θ is the volumetric water content, t is time, h denotes the pressure head, K is the hydraulic conductivity tensor, and z represents the vertical coordinate. $C(h) = \frac{\partial \theta}{\partial h}$ is the hydraulic capacity and $D(\theta)$ introduces diffusivity [8].

2.1 Constitutive models for unsaturated soil

The constitutive models employed in this study are the Brooks– Corey's [28] and the Mualem-van Genuchten's (MG) models [29]. It should be indicated that these models present the hydraulic behaviour of unsaturated soils.

2.1.1 Brooks-Corey's model

The Brooks-Corey's model is expressed by:

$$\theta = \theta_r + (\theta_s - \theta_r)\left(\frac{h}{h_e}\right)^{-\lambda} \tag{4}$$

$$K(h) = K_s\left(\frac{h}{h_d}\right)^{-2-3\lambda} \tag{5}$$

where θ_r and θ_s are the residual and saturated water content, respectively. K_s is the saturated hydraulic conductivity, h_d denotes the air entry pressure head, and λ is the pore size distribution index of the model [28].

2.1.2 Mualem-van Genuchten's model

The Mualem-van Genuchten function reads [29]:

$$S_e = \frac{\theta - \theta_r}{\theta_s - \theta_r} = \frac{1}{(1+(\alpha|h|)^n)^m} \tag{6}$$

$$K = K_s {S_e}^{0.5}\left(1-\left(1-{S_e}^{1/m}\right)^m\right)^2 \tag{7}$$

in which S_e is the effective saturation, α is inversely propotional to h_d, n denotes the pore size distribution parameter and $m = 1 - 1/n$.

3. Numerical models

In the following sections, the Dual-Discrete finite volume method has been applied to discretize the different forms of the Richards' equation.

3.1 Numerical discretization of the h-based form

By integrating Equation 2 over a control volume Ω_i and neglecting gravity, yields:

$$\int_{\Omega_i}\left(C\frac{\partial h}{\partial t} - \nabla(K\nabla h)\right)d\Omega = 0 \tag{8}$$

By implementing the Gauss-Green theorem, the above equation can be written as follows:

$$\int_{\Omega_i}\left(C\frac{\partial h}{\partial t}\right)d\Omega - \int_{\partial\Omega_i}\mathbf{n}.(K\nabla h)\,d\Gamma = 0 \tag{9}$$

in which, $\partial\Omega_i$ is the control volume boundary and **n** is the corresponding normal vector. The discretized form of the above equation could be expressed as follows:

$$C\frac{\partial h_i}{\partial t}|\Omega_i| + \sum_{\Gamma_{ij}\epsilon\,\partial\Omega_i} V_{ij}|\Gamma_{ij}| = 0 \tag{10}$$

in the above equation h_i is the pressure head at the cell-center, Γ_{ij} is the interface between two neighbor cells of Ω_i and Ω_i ($\Omega_i \cap \Omega_j = \Gamma_{ij}$) and V_{ij} is the flux at this interface. The flux term V_{ij} could be defined as follows:

$$V_{ij} = -\frac{1}{|\Gamma_{ij}|}\int_{\Gamma_{ij}} \mathbf{n}.(K\nabla h)\, d\Gamma \tag{11}$$

To evaluate the above integration, the following equation has been used for the pressure gradient at the cell edge Γ_{ij} [20, 22, 30-32]:

$$\boldsymbol{\psi_{ij}} = \left(\frac{h_j - h_i}{D_{ij}} - \cot\alpha \frac{h_J - h_I}{|\Gamma_{ij}|}\right)\mathbf{n_{ij}} + \frac{h_J - h_I}{|\Gamma_{ij}|}\mathbf{t_{ij}} \tag{12}$$

where h_i and h_j are the head values at the triangle centers of i and j, respectively. Also h_I and h_J denote the head values at the vertices, I and J, respectively. Other parameters are shown in Fig. 1.

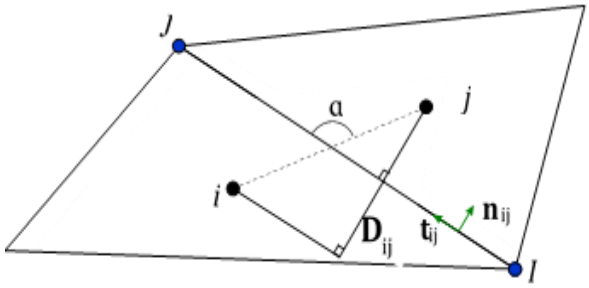

Fig. 1: The parameters used in the DDFVM

By implementing equation 12 in equation 11, the following form for the numerical flux could be obtained [20, 22, 30-32]:

$$V_{ij} = -\kappa_{nn}\frac{h_j - h_i}{D_{ij}} - (\kappa_{nt} - \cot\alpha\kappa_{nn})\frac{h_J - h_I}{|\Gamma_{ij}|} \tag{13}$$

where κ_{nn} and κ_{nt} are the hydraulic conductivity components in the local coordinate of $(n_{ij}.t_{ij})$. The unknown values h_I and h_J would be approximated by the least square method [20, 22, 30-32]. Finally, the discrete form could be derived by introducing equation 13 into equation 10.

3.2 Numerical discretization of the θ-based form

In a similar manner, by integrating the θ- form of Richards' equation, we have:

$$\int_{\Omega_i}\left(\frac{\partial\theta}{\partial t} - \nabla(D_\theta\nabla\theta)\right)d\Omega = 0 \tag{14}$$

$$\int_{\Omega_i}\frac{\partial\theta}{\partial t}d\Omega - \int_{\partial\Omega_i}\mathbf{n}.(D_\theta\nabla\theta)\,d\Gamma = 0 \tag{15}$$

$$\frac{\partial\theta_i}{\partial t}|\Omega_i| + \sum_{\Gamma_{ij}\epsilon\,\partial\Omega_i} V_{ij}|\Gamma_{ij}| = 0 \tag{16}$$

in the above equation θ_i represents the water content value at the cell center i. For the θ- form, the parameter V_{ij} is given by:

$$V_{ij} = -\frac{1}{|\Gamma_{ij}|}\int_{\Gamma_{ij}}\mathbf{n}.(D_\theta\nabla\theta)\,d\Gamma \tag{17}$$

To discretize equation 17, the water content gradient between two neighbor cells has been expressed as follows:

$$\zeta_{ij} = \left(\frac{\theta_j - \theta_i}{D_{ij}} - \cot\alpha\frac{\theta_J - \theta_I}{|\Gamma_{ij}|}\right)n_{ij} + \frac{\theta_J - \theta_I}{|\Gamma_{ij}|}t_{ij} \tag{18}$$

in which θ_i and θ_j are the water content values at the control volume centers of i and j, respectively, while θ_I and θ_J are the corresponding values at the vertices shown in Fig. 1.

Applying equation 18 in equation 17 leads to the following equation:

$$V_{ij} = -\xi\zeta_{ij}.\mathbf{n}_{ij} \tag{19}$$

where ξ could be determined as follows:

$$\xi = \frac{1}{|\Gamma_{ij}|}\int_{\Gamma_{ij}} D_\theta\, d\Gamma = \begin{bmatrix}\xi_{nn} & \xi_{nt}\\ \xi_{tn} & \xi_{tt}\end{bmatrix} \text{ in } (n_{ij}.t_{ij}) \tag{20}$$

Considering equations 18 - 20, equation 17 could be written as:

$$V_{ij} = -\xi_{nn}\frac{\theta_j - \theta_i}{D_{ij}} - (\xi_{nt} - \cot\alpha\xi_{nn})\frac{\theta_J - \theta_I}{|\Gamma_{ij}|} \tag{21}$$

The water content values at the vertices could be calculated by the following equation:

$$\theta_I = \sum_{i=1}^{N_I} w_i(\theta_i) \tag{22}$$

where w_i has been computed from the least square method [20, 22, 30-32] and N_I is the number of cells around the point I. By substituting equations 21 and 22 into equation 13, the θ-based form could be discretized.

3.3 Numerical discretization of the mixed form

Following a similar procedure, the mixed form of Richards' equation could be written as follows:

$$\int_{\Omega_i}\left(\frac{\partial\theta}{\partial t} - \nabla.K\nabla h\right)d\Omega = 0 \tag{23}$$

$$\int_{\Omega_i}\left(\frac{\partial\theta}{\partial t}\right)d\Omega - \int_{\partial\Omega_i}\mathbf{n}.(K\nabla h)\,d\Gamma = 0 \tag{24}$$

With the modified Picard approximation, the time derivative of water content can be provided as follows [8]:

$$\int_{\Omega_i}\left(\frac{\partial\theta}{\partial t}\right)d\Omega=\frac{\partial\theta_i}{\partial t}|\Omega_i|=\left(\frac{{\theta_i}^{n+1.k}-{\theta_i}^{n}}{\Delta t}\right)|\Omega_i| \approx\frac{{\theta_i}^{n+1.k}+{C_i}^{n+1.k}({h_i}^{n+1.k+1}-{h_i}^{n+1.k})-{\theta_i}^{n}}{\Delta t}|\Omega_i| \quad (25)$$

in the above equation, n is the time level, k is the iteration number, and Δt represents the time step. Since in equation 25, the unknown parameter is the hydraulic head, the second term in equation (24) has been discretized similarly to the h-based form.

3.4 The algorithms for different forms of Richards' equation

The following algorith has been applied for the different forms:

Step 1. Set $\theta^{n+1.1}=\theta^{n}$ *and* $h^{n+1.1}=h^{n}$

Step 2. For k=1, 2, …UNTIL CONVERGENCE

IF h-based form or mixed form

Calculate ${C_i}^{n+1.k+1}$ and ${K_i}^{n+1.k+1}$

Solve ${h_i}^{n+1.k+1}$

ELSE

Calculate ${D_i}^{n+1.k+1}$

Solve ${\theta_i}^{n+1.k+1}$

END

Step 3. Go to step 1 for the next time step

4. Results

In the following section, the numerical model of DDFVM has been validated via different examples, and different forms of Richards' equation have been compared according to the mass balance ratio, iteration, and relative error.

4.1 Example 1

The details of this example are adapted from [33]. A soil column of 1 cm in width and 20 cm in length has been considered. The initial moisture content for all points of the specimen is 0.2. As it is illustrated in Fig. 2, the boundary condition at the top and bottom are of Neuman type, and at the left and right boundaries, the Dirichlet boundary condition is applied. The moisture content at the left edge is equal to 0.45, while it is equal to 0.2 at the right boundary. The other required details are given hereafter:

$$k(\theta)=\frac{10\theta}{3}-0.5\ \mathrm{cm/day} \quad (26)$$

$$h=\frac{10^3\theta}{3}-150\mathrm{cm} \quad (27)$$

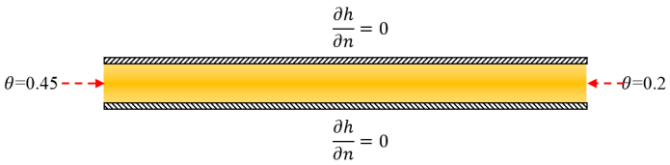

Fig. 2: The boundary conditions of the first example

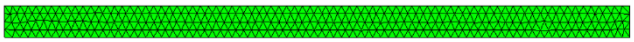

Fig. 3: The unstructured mesh for the first example based om Delaunay triangulation

The unstructured mesh of the problem that is generated by Netgen software is shown in Fig. 3. The mesh size has been selected to be equal to 0.5 cm, and the problem domain is discretized to 640 elements and 405 nodes. In the sequel, numerical results of the moisture content are given for both 1D and 2D models at time lapses T=0.01 day and T=0.06 day. The time step for this problem is set to 0.00005 day.

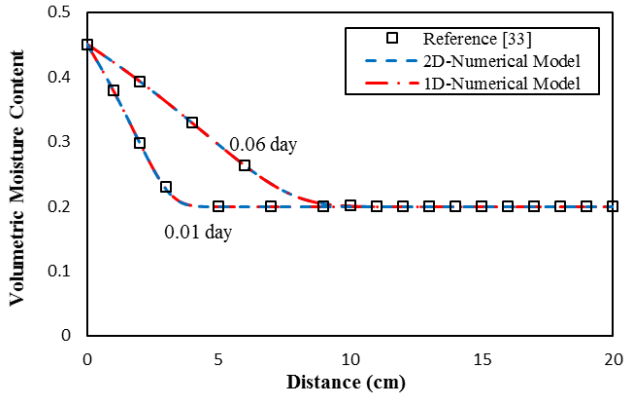

Fig. 4: The variation of water content at different time lapses

In this example, due to a lack of data, it was impossible to attain results based on head and modified Picard forms. The acquired outcomes from the mass balance in the form of moisture content indicate that by increasing the time step, the error in mass balance slightly improves; the reason for such an observance is that at the first time step, there is an inconsistency between the boundary and initial conditions that yields to an error in mass balance.

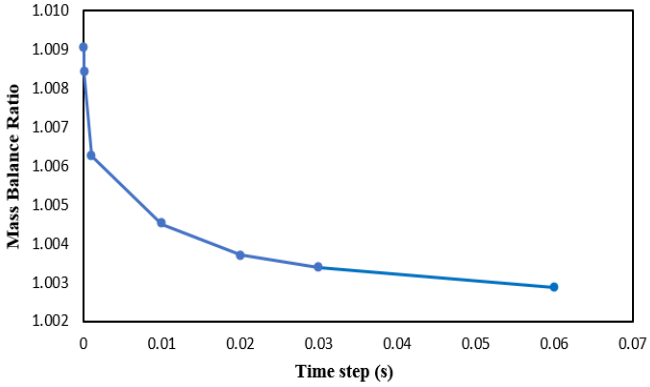

Fig. 5: The mass balance ratio for different time steps

4.2 Example 2

The second example is a slightly modified example adapted from [34] and used for verification under drainage condition. The initial head and moisture content are read to be 4 cm and 0.41, respectively. The top and bottom boundary conditions are of Neumann type, while boundary conditions at the left and right boundaries are set to Dirichlet type. The head and moisture content at the left boundary are 4 cm and 0.4, and at the right boundary are 6.308 cm and 0.3, respectively. The problem data are given in Table 1, and the mesh layout is given in Fig. 6. The mesh size is set to 0.5 in the Netgen software resulting in a mesh with 318 elements and 242 nodes. It should be indicated that the Brooks-Corey's constitutive model has been employed in this problem and the soil type is fine sand [34].

Table 1: The parameters of the second example

Parameter		Values
Residual water content	θ_r $(cm^3 cm^{-3})$	0.03
Saturated Water content	θ_s $(cm^3 cm^{-3})$	0.41
Hydraulic conductivity	K_s $(cm\ h^{-1})$	0.24
Constant parameter	n	0.75
Constant parameter	m	4.25
Air entry suction head	h_d	4

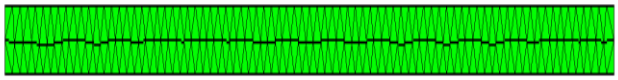

Fig. 6: The unstructured mesh for the second example based om Delaunay triangulation

The numerical results for the three methods are shown in Fig. 7 at time lapses of T=150 min and T=650 min. The size of the time step in this example is equal to 10 min.

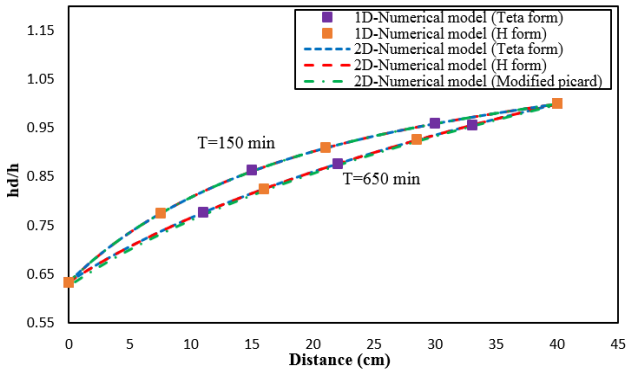

(a)

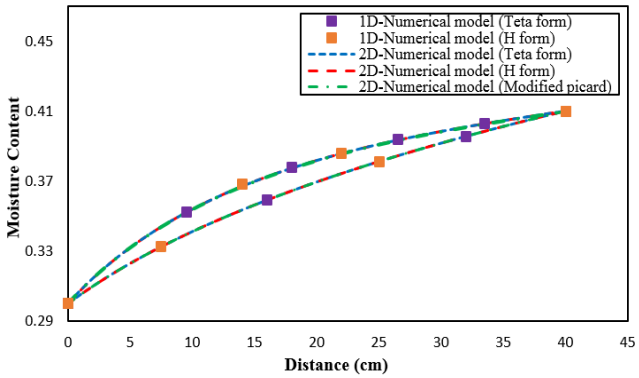

(b)

Fig. 7: (a) The variation of dimensionless head vs. distance; (b) The variation of moisture content vs. distance.

The total number of iterations for different values of acceptable error are attained for the three forms based on head, moisture content, and mixed modified Picard. By comparing the total number of iterations given in Table 2, the θ-based form shows superior performance. Also the allowable error for the h-based, mixed forms and θ-based form are defined as follows:

- h-based and mixed forms

$$\text{Allowable error} = max\left(\frac{h_i^{n+1.k+1} - h_i^{n+1.k}}{h_i^{n+1.k+1}}\right)$$

- θ-based form

$$\text{Allowable error} = max\left(\frac{\theta_i^{n+1.k+1} - \theta_i^{n+1.k}}{\theta_i^{n+1.k+1}}\right)$$

Table 2: The total number of iterations for the three forms h-based, θ-based, and modified Picard

Method	Allowable error=0.001	Allowable error=0.0001	Allowable error=0.00001
-based θ form	103	142	192
h-based form	111	162	223
Modified Picard	112	161	221

Furthermore, it is shown in Fig. 8 that the mass balance ratio in the θ-based form is giving more promising results compared to the other two forms. However, using the modified Picard form properly yields the conservation of mass balance law. Also, the head-based method will result in a better mass balance at the smaller time steps, while increasing the size of time step increases mass balance errors.

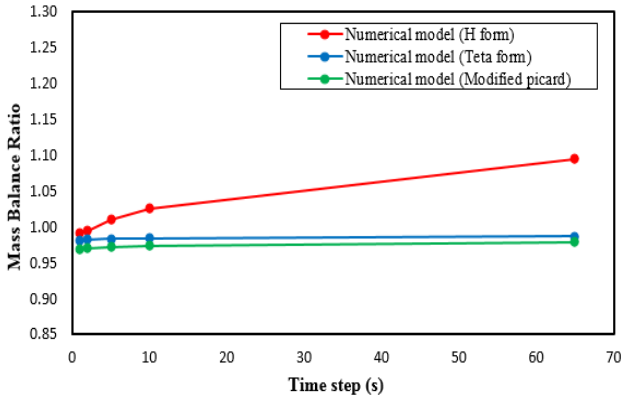

Fig. 8: The mass balance ratio vs. time step for the three forms h-based, θ-based, and modified Picard

4.3 Example 3

In the third example, a horizontal soil strip with a width of 1 cm and length of 100 cm is modelled [35]. The initial head and moisture content are equal to -1711.52 cm and 0.113, respectively. The no-flow boundary conditions are applied at the top and bottom. The values for the head and moisture content are assumed to be -1711.52 cm and 0.113 for the left boundary, and 0 cm and 0.43 at the right boundary, respectively. The other parameters are listed in Table. 3.

Table 3: The parameters of the third example

Parameter		Values
Residual water content	θ_r (cm^3cm^{-3})	0.078
Saturated Water content	θ_s (cm^3cm^{-3})	0.43
Hydraulic conductivity	K_s $(cm\ min^{-1})$	0.0173
Constant parameter	n	1.56
Constant parameter	m	0.359
Air entry pressure index	$\alpha(cm^{-1})$	0.036

In this example, the structured triangular mesh has been implemented. The grid size is set to be 0.5 cm, resulting in a mesh of 800 elements and 603 nodes. Additionally, the Mualem-van Genuchten model has been used for the silty soil of this example. Numerical results of the h-based, θ-based, and mixed modified Picard at the time lapses of T=250, 800, and 1200 min are depicted in the following figures.

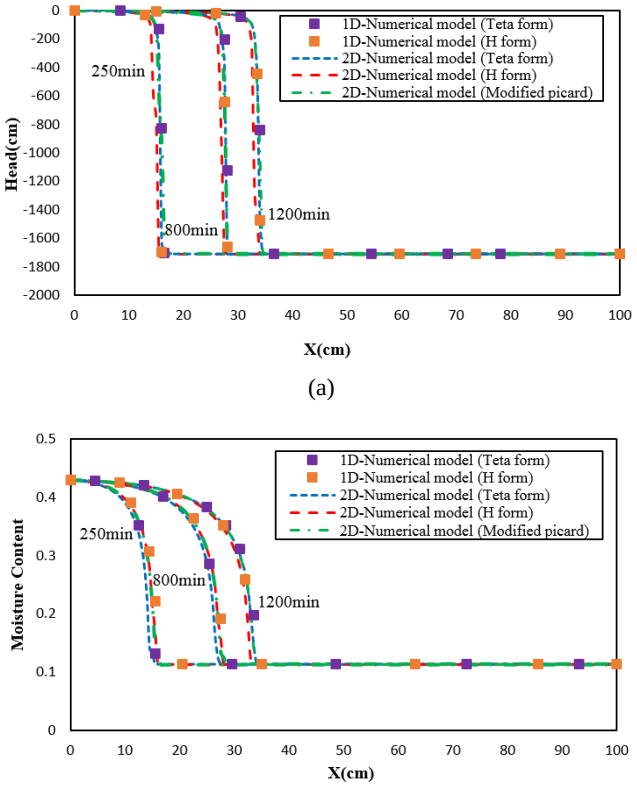

Fig. 9: (a) The variation of head along the length; (b) The variation of moisture content along the length.

In this problem, at T=800 min, the iterations are chosen to be equal to 5 for the three forms, and the errors are compared as follows:

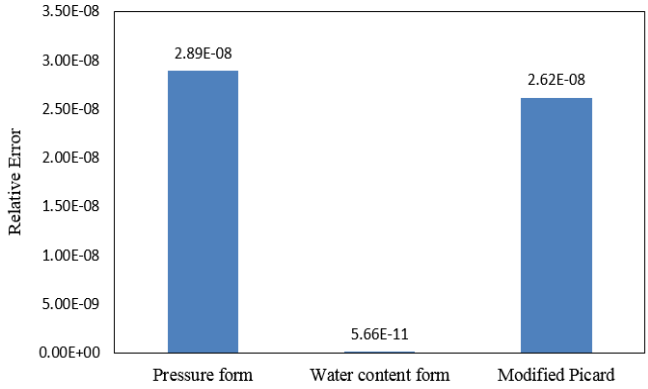

Fig. 10: The relative error for the three forms of h-based, θ-based, and modified Picard

As shown in Fig.10, the relative error of form θ-based is less in comparison to the modified Picard, while the modified Picard yields a lower error than the h-based form. Thus, it can be concluded that the θ-based form results in higher precision. Furthermore, the RMSE values for different schemes are listed in Table 4 at T=800 min. According to this table, the h-based scheme shows the highest values of RMSE in both parameters of water content and head.

Table 4: The RMSE values for different schemes

Scheme	RMSE-θ	RMSE-h (cm)
h-based	0.008	94.511
θ- based	0.007	39.649
Mixed form	0.006	50.021

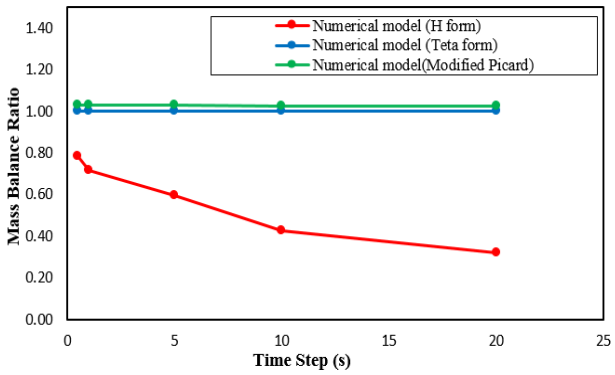

Fig. 11: The mass balance ratio vs. time step for the three forms h-based, θ-based, and modified Picard

It can be observed from Fig. 11 that the mass balance ratio in the θ-based form gives more reliable results when compared to the other two forms. Again, in this example, the mass balance error will increase when greater time steps are implemented in the h-based form.

4.4 Example 4

The parameters and geometry of this problem are extracted from [36]. A soil layer of 1 cm width and 200 cm length is considered which is comprised of two different soils (Fig.12). The initial condition for head is assumed to be -50 cm. The boundary conditions at the top, bottom and right are no-flow, while the boundary conditions at the left boundary is head prescribed. The head and moisture content at the left boundary set to -16 cm and 0.294, respectively. The initial conditions are as follows:

$h_{Medium\ sand}(x.0) = -50.207; h_{Fine\ sand}(x.0) = -49.98$

$\theta_{Medium\ sand}(x.0) = 0.043; \theta_{Fine\ sand}(x.0) = 0.169$

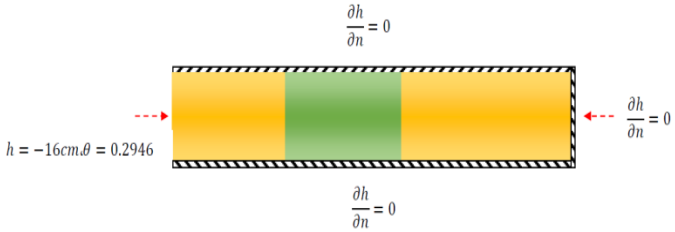

Fig. 12: The boundary conditions and set-up of the fourth example

Moreover, the mesh size is considered 0.5 cm corresponding to a discretized domain of 1600 elements and 1203 nodes. The other parameters for the two types of soil are listed in Table. 5. The numerical results for the three forms are given at time T=7918 s in Fig. 13.

Table 5: The parameters of the fourth example

Medium sand		
Parameter		**Values**
Intrinsic permeability	k	10^{-7}
Porosity	φ	0.35
Air entry pressure head	h_d	15
Residual saturation	s_r	0.1
Pore size distribution index	λ	3
Fine sand		
Parameter		**Values**
Intrinsic permeability	k	10^{-9}
Porosity	φ	0.35
Air entry pressure head	h_d	25
Residual saturation	s_r	0.2
Pore size distribution index	λ	1.5

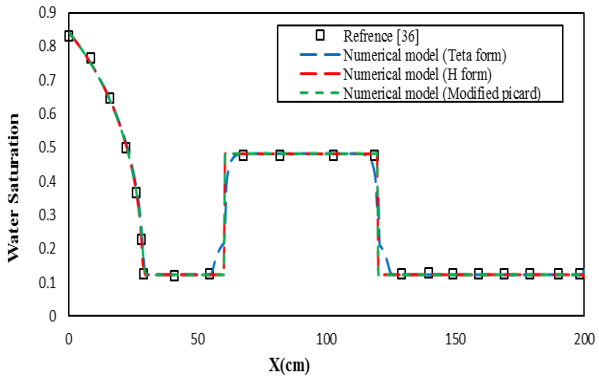

Fig. 13: (a) The variation of water saturation along the length at T=7918 s

As presented in Table.6, in a multi-layered soil example similar to the previous problems, the θ-based form needs fewer iterations to converge. Moreover, the mass balance ratio in the θ-based form leads to superior results than the other two forms (Fig. 14). As illustrated in Fig.14, the θ-based form is found to give appropriate mass balance ratio error even for the case of greater time steps, so, the above-mentioned points approves the superiority of θ-based form over the two other schemes for the case of multi-layered soils. Additionally, between the two methods of modified Picard and h-based, the scheme of modified Picard demonstrates higher computational speed, lower error, and higher mass balance precision.

Table 6: The total number of iterations for the three forms h-based, θ-based, and modified Picard

Method	Allowable error=0.001	Allowable error=0.0001	Allowable error=0.00001
-based θ form	2566	3145	3929
h-based form	2757	3642	4606
Modified Picard	2660	3442	4383

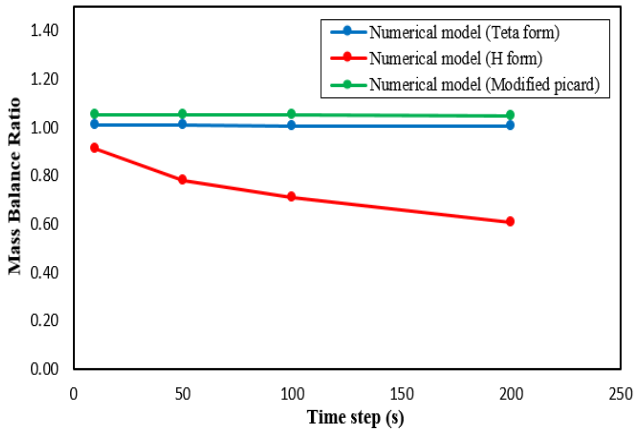

Fig. 14: The mass balance ratio vs. time step for the three forms h-based, θ-based, and modified Picard

4.5 Example 5

To investigate the methods in a two-dimensional flow problem, the example in [34] has been modified, as shown in Fig. 15.

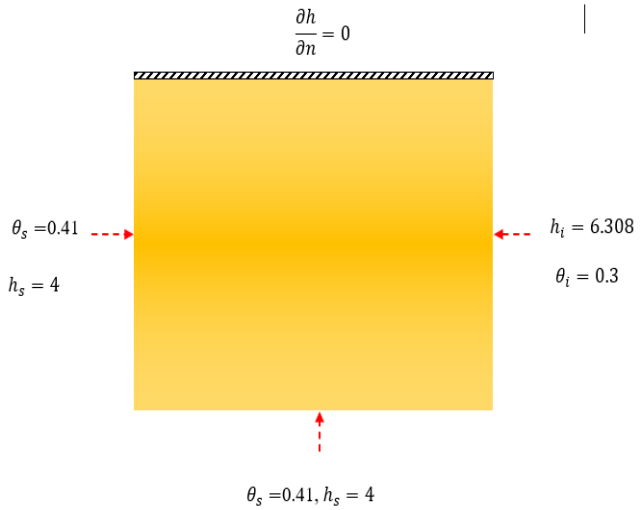

Fig. 15: The boundary conditions of the fifth example

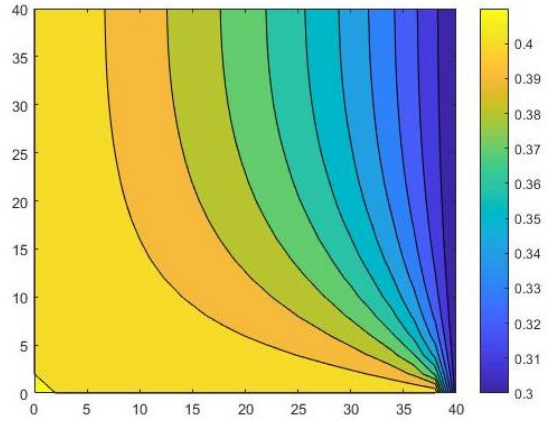

(a)

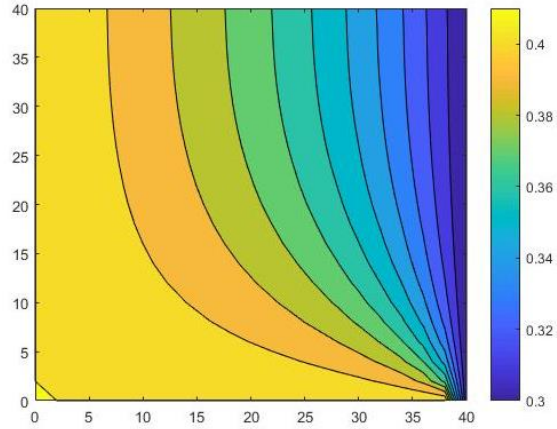

(b)

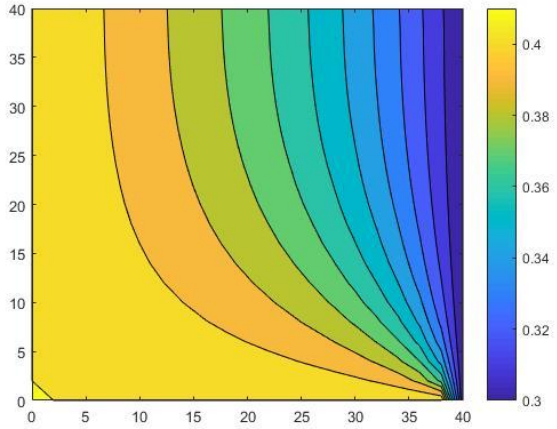

(c)

Fig. 16: The moisture content at T=600 min for (a) the θ-based form, (b) the h-based form, (c) the modified Picard

An unsaturated soil with a depth and height of 40 cm is considered. The initial head and moisture content are read to be equal to 6.308 cm and 0.3, respectively. The boundary conditions are shown in Fig.15. For this problem, the structured triangular mesh with the size of 2 cm has been considered, resulting in 800 elements and 441 nodes. The soil properties are similar to Table.1, and the Brooks-Corey's model has been employed. The results for the

moisture content for the three forms are shown in Fig. 16 at time T=600 min.

By comparing the total iterations in Table 7, and the mass balance ratio of different form in Fig. 17, it is evident that the θ-based scheme needs fewer iterations with higher accuracy, thus, is a more appropriate scheme.

Table 7: The total number of iterations for the three forms h-based, θ-based, and modified Picard

Method	Allowable error=0.001	Allowable error=0.0001	Allowable error=0.00001
-based θ form	737	893	1029
h-based form	765	929	1200
Modified Picard	766	932	1200

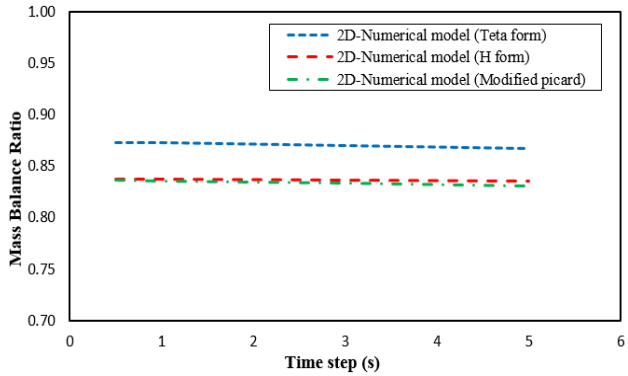

Fig. 17: The mass balance ratio vs. time step for the three forms h-based, θ-based, and modified Picard

5. Conclusions

In this research, the advanced finite volume scheme of the Dual Discrete method has been used for numerical modeling of Richards' equation. Three forms of Richards' equation, including head form, water content form, and mixed form with a modified Picard linearization, are developed and assessed in two-dimensional domain. Various examples using different soil properties, boundary conditions and grid structures are solved. The results agree very well with the analytical and numerical solutions in both homogenous and layered porous media. The different forms have been compared in terms of accuracy, the number of iterations, and mass balance ratio. For the test cases considered in this study, the water content form has been determined as the superior method due to the low mass balance error, higher accuracy, and less number of iterations. The total number of iterations in the water content form decreases between 7 to 14% in comparison with the two other schemes. Also, the modified Picard form improves conservation of mass and efficiency in comparison to the head-based method. The results indicate that for the head form, a small time step is required to obtain an accurate mass balance, and for larger time steps, the mass balance error increases. Contrary to the head form, the two other schemes yield superior mass balance results, even for large time steps. Based on the examples solved in this paper, the mass balance error for the water content form is between -13% to 1%, for the mixed form is in the range of -17% to 5% and for the h-based form the error inreval increases to -68% - 10%. Moreover, the DDFVM shows stable solutions without any numerical oscillations for all examples.

References

[1] Farthing, M. W., & Ogden, F. L. (2017). Numerical solution of Richards' equation: A review of advances and challenges. *Soil Science Society of America Journal*, *81*(6), 1257-1269.

[2] Zhang, Z., Wang, W., Yeh, T.C.J., Chen, L., Wang, Z., Duan, L., An, K. & Gong, C. (2016). Finite analytic method based on mixed-form Richards' equation for simulating water flow in vadose zone. *Journal of hydrology*, *537*, 146-156.

[3] Taigbenu, A. E., & Onyejekwe, O. O. (1995). Green element simulations of the transient nonlinear unsaturated flow equation. *Applied mathematical modelling*, *19(11)*, 675-684.

[4] Richards, L. A. (1931). Capillary conduction of liquids through porous mediums. *Physics*, *1(5)*, 318-333.

[5] Forsyth, P. A., Wu, Y. S., & Pruess, K. (1995). Robust numerical methods for saturated-unsaturated flow with dry initial conditions in heterogeneous media. *Advances in Water Resources*, *18(1)*, 25-38.

[6] Romano, N., Brunone, B., & Santini, A. (1998). Numerical analysis of one-dimensional unsaturated flow in layered soils. *Advances in Water Resources*, *21*(4), 315-324.

[7] Ross, P. J. (2003). Modeling soil water and solute transport-Fast, simplified numerical solutions. *Agronomy journal*, *95(6)*, 1352-1361.

[8] Celia, M. A., Bouloutas, E. T. & Zarba, R. L. (1990). A general mass-conservative numerical solution for the unsaturated flow equation. *Water resources research*, 26, 1483-1496.

[9] Kirkland, M. R., Hills, R. & Wierenga, P. (1992). Algorithms for solving Richards' equation for variably saturated soils. *Water Resources Research*, 28, 2049-2058.

[10] Manzini, G. & Ferraris, S. (2004). Mass-conservative finite volume methods on 2-D unstructured grids for the Richards' equation. *Advances in Water Resources*, 27, 1199-1215

[11] Caviedes-Voullième, D., Garcı, P. & Murillo, J. (2013). Verification, conservation, stability and efficiency of a finite

volume method for the 1D Richards equation. *Journal of hydrology*, 480, 69-84.

[12] Berardi, M., Difonzo, F. & Lopez, L. (2020). A mixed MoL–TMoL for the numerical solution of the 2D Richards' equation in layered soils. *Computers & Mathematics with Applications*, *79*(7), 1990-2001.

[13] Farahi, G., Khodashenas, S.R., Alizadeh, A. & Ziaei, A.N. (2017). New model for simulating hydraulic performance of an infiltration trench with finite-volume one-dimensional Richards' equation. *Journal of Irrigation and Drainage Engineering*, *143*(8), 04017025.

[14] Younes, A., Fahs, M. & Belfort, B. (2013). Monotonicity of the cell-centred triangular MPFA method for saturated and unsaturated flow in heterogeneous porous media. *Journal of hydrology*, 504, 132-141.

[15] Milly, P. 1984. A mass-conservative procedure for time-stepping in models of unsaturated flow. *Finite elements in water resources.* Springer.

[16] Karthikeyan, M., Tan, T. S., & Phoon, K. K. (2001). Numerical oscillation in seepage analysis of unsaturated soils. *Canadian geotechnical journal*, *38*(3), 639-651.

[17] Pan, L., Warrick, A. W., & Wierenga, P. J. (1996). Finite element methods for modeling water flow in variably saturated porous media: Numerical oscillation and mass-distributed schemes. *Water Resources Research*, *32*(6), 1883-1889.

[18] Asadi, R., Ataie-Ashtiani, B., & Simmons, C. T. (2014). Finite volume coupling strategies for the solution of a Biot consolidation model. *Computers and Geotechnics*, *55*, 494-505.

[19]Asadi, R. & Ataie-Ashtiani, B. (2015). A comparison of finite volume formulations and coupling strategies for two-phase flow in deforming porous media. *Computers and Geotechnics*, 67, 17-32.

[20] Asadi, R. and Ataie-Ashtiani, B., (2016). Numerical modeling of subsidence in saturated porous media: A mass conservative method. *Journal of hydrology*, *542*, pp.423-436.

[21] Asadi, R. (2018). A Mass Conservative Method for Numerical Modeling of Axisymmetric flow. *Journal of Hydraulic Structures*, *4*(2), 1-9.

[22] Asadi, R., & Ataie-Ashtiani, B. (2021). Hybrid finite volume-finite element methods for hydro-mechanical analysis in highly heterogeneous porous media. *Computers and Geotechnics*, *132*, 103996.

[23] Droniou, J. (2014). Finite volume schemes for diffusion equations: introduction to and review of modern methods. *Mathematical Models and Methods in Applied Sciences*, *24*(08), 1575-1619.

[24] Crevoisier, D., Chanzy, A., & Voltz, M. (2009). Evaluation of the Ross fast solution of Richards' equation in unfavourable conditions for standard finite element methods. *Advances in water resources*, *32*(6), 936-947.

[25] Warrick, A. W. (1991). Numerical approximations of Darcian flow through unsaturated soil. *Water Resources Research*, *27*(6), 1215-1222.

[26] van Dam, J. C., Groenendijk, P., Hendriks, R. F., & Kroes, J. G. (2008). Advances of modeling water flow in variably saturated soils with SWAP. *Vadose Zone Journal*, *7*(2), 640-653.

[27] Šimůnek, J., van Genuchten, M. T., & Šejna, M. (2008). Development and applications of the HYDRUS and STANMOD software packages and related codes. *Vadose Zone Journal*, *7*(2), 587-600.

[28] Brooks, R.H., Corey, A.T. (1965). *Hydraulic properties of porous media*. Colorado State University.

[29] Van Genuchten, M. T. (1980). A closed-form equation for predicting the hydraulic conductivity of unsaturated soils. *Soil science society of America journal*, *44*(5), 892-898.

[30] Coudière, Y., Vila, J. P., & Villedieu, P. (1999). Convergence rate of a finite volume scheme for a two dimensional convection-diffusion problem. *ESAIM: Mathematical Modelling and Numerical Analysis*, *33*(3), 493-516.

[31] Coudière, Y., & Villedieu, P. (2000). Convergence rate of a finite volume scheme for the linear convection-diffusion equation on locally refined meshes. *ESAIM: Mathematical Modelling and Numerical Analysis*, *34*(6), 1123-1149.

[32] Bevilacqua, I., Canone, D., & Ferraris, S. (2011). Acceleration techniques for the iterative resolution of the Richards equation by the finite volume method. *International Journal for Numerical Methods in Biomedical Engineering*, *27*(8), 1309-1320.

[33] Taigbenu, A.E. & Onyejekwe, O.O. (1995). Green element simulations of the transient nonlinear unsaturated flow equation. *Applied mathematical modelling*, *19*(11), 675-684.

[34] Wang, Q., Horton, R. & Shao, M. (2002). Horizontal infiltration method for determining Brooks-Corey model parameters. *Soil Science Society of America Journal*, *66*(6), 1733-1739.

[35] Sayah, B., Gil-Rodríguez, M. & Juana, L. (2016). Development of one-dimensional solutions for water infiltration. Analysis and parameters estimation. *Journal of Hydrology*, *535*, 226-234.

[36] Marinelli, F. & Durnford, D.S. (1998). Semianalytical solution to Richards' equation for layered porous media. *Journal of irrigation and drainage engineering*, *124*(6), 290-299.